

# Earth and Space Science



## RESEARCH ARTICLE

10.1029/2021EA002069

### Key Points:

- ~20% of the ocean floor topography has been surveyed by ships, the remaining 80% is predicted by satellite altimetry
- We increased the resolution of the predicted depth using spectral properties of abyssal hills and the characteristic shapes of seamounts
- We estimate the height and radius of 19,000 uncharted seamounts

### Correspondence to:

D. T. Sandwell,  
dsandwell@ucsd.edu

### Citation:

Sandwell, D. T., Goff, J. A., Gevorgian, J., Harper, H., Kim, S.-S., Yu, Y., et al. (2022). Improved bathymetric prediction using geological information: SYNBATH. *Earth and Space Science*, 9, e2021EA002069. <https://doi.org/10.1029/2021EA002069>

Received 8 OCT 2021  
Accepted 4 JAN 2022

### Author Contributions:

**Conceptualization:** David T. Sandwell, John A. Goff, Julie Gevorgian, Seung-Sep Kim, Paul Wessel, Walter H. F. Smith  
**Formal analysis:** David T. Sandwell, John A. Goff, Hugh Harper, Paul Wessel, Walter H. F. Smith

**Funding acquisition:** David T. Sandwell

**Methodology:** David T. Sandwell, John A. Goff, Julie Gevorgian, Hugh Harper, Seung-Sep Kim, Yao Yu, Brook Tozer, Paul Wessel, Walter H. F. Smith

**Project Administration:** David T. Sandwell

**Software:** David T. Sandwell, John A. Goff, Julie Gevorgian, Hugh Harper, Yao Yu, Brook Tozer, Paul Wessel, Walter H. F. Smith

**Supervision:** David T. Sandwell

© 2022 The Authors. *Earth and Space Science* published by Wiley Periodicals LLC on behalf of American Geophysical Union.

This is an open access article under the terms of the [Creative Commons Attribution License](#), which permits use, distribution and reproduction in any medium, provided the original work is properly cited.

## Improved Bathymetric Prediction Using Geological Information: SYNBATH

David T. Sandwell<sup>1</sup> , John A. Goff<sup>2</sup> , Julie Gevorgian<sup>1</sup>, Hugh Harper<sup>1</sup> , Seung-Sep Kim<sup>3</sup> , Yao Yu<sup>1</sup>, Brook Tozer<sup>4</sup>, Paul Wessel<sup>5</sup> , and Walter H. F. Smith<sup>6</sup>

<sup>1</sup>Scripps Institution of Oceanography, University of California San Diego, La Jolla, CA, USA, <sup>2</sup>Jackson School of Geosciences, Institute for Geophysics, University of Texas at Austin, Austin, TX, USA, <sup>3</sup>Department of Geological Sciences, Chungnam National University, Daejeon, Korea, <sup>4</sup>GNS Science, Wellington, New Zealand, <sup>5</sup>Department of Earth Sciences, SOEST, University of Hawaii at Manoa, Honolulu, HI, USA, <sup>6</sup>Laboratory for Satellite Altimetry, NOAA, College Park, MD, USA

**Abstract** To date, ~20% of the ocean floor has been surveyed by ships at a spatial resolution of 400 m or better. The remaining 80% has depth predicted from satellite altimeter-derived gravity measurements at a relatively low resolution. There are many remote ocean areas in the southern hemisphere that will not be completely mapped at 400 m resolution during this decade. This study is focused on the development of synthetic bathymetry to fill the gaps. There are two types of seafloor features that are not typically well resolved by satellite gravity; abyssal hills and small seamounts (<2.5 km tall). We generate synthetic realizations of abyssal hills by combining the measured statistical properties of mapped abyssal hills with regional geology including fossil spreading rate/orientation, rms height from satellite gravity, and sediment thickness. With recent improvements in accuracy and resolution, it is now possible to detect all seamounts taller than about 800 m in satellite-derived gravity and their location can be determined to an accuracy of better than 1 km. However, the width of the gravity anomaly is much greater than the actual width of the seamount so the seamount predicted from gravity will underestimate the true seamount height and overestimate its base dimension. In this study, we use the amplitude of the vertical gravity gradient (VGG) to estimate the mass of the seamount and then use their characteristic shape, based on well-surveyed seamounts, to replace the smooth-predicted seamount with a seamount having a more realistic shape.

**Plain Language Summary** The floor of the deep ocean remains as the last uncharted frontier in the inner solar system. The deep seawater (>1,000 m) prevent any type of exploration from conventional satellite remote sensing. Echosounders aboard large vessels have mapped about 20% of the seafloor, however, vast areas in the southern hemisphere will not be mapped in our lifetimes. The deep ocean floor has more than 90% of the active volcanoes; hydrothermal circulation of seawater through the crust of the seafloor spreading ridges replenishes the nutrients needed for life on Earth. This study is an effort to fill the large gaps in seafloor coverage by creating a synthetic abyssal hill fabric using geological information such as the age of the seafloor, the spreading rate and direction when it formed, and the thickness of the sediments covering the original topography. In addition, we use the latest satellite-derived gravity to estimate the locations and shapes of about 20,000 uncharted seamounts. The combination of mapped (20%) and synthetic (80%) topography is useful for modeling ocean circulation and ocean tides although it may give a false impression that 100% of the seafloor has been mapped.

## 1. Introduction

Bathymetry is foundational data, providing basic infrastructure for scientific, economic, educational, military, and political work. High resolution, deep ocean bathymetry is critical for: (a) understanding the geologic processes responsible for creating ocean floor features unexplained by simple plate tectonics, such as abyssal hills, seamounts, microplates, propagating rifts, and intraplate deformation; (b) determining the effects of bathymetry and seafloor roughness on ocean circulation, ocean mixing, and climate; and (c) understanding how marine life is influenced by seafloor depth, roughness, and interactions of currents with the seafloor (Yesson et al., 2011). The Seabed 2030 project (<https://seabed2030.org>) “aims to bring together all available bathymetric data to produce the definitive map of the world ocean floor by 2030 and make it available to all.” The Seabed 2030 global

**Writing – original draft:** David T.

Sandwell, Julie Gevorgian

**Writing – review & editing:** John A.

Goff, Julie Gevorgian, Hugh Harper,

Seung-Sep Kim, Yao Yu, Paul Wessel,

Walter H. F. Smith

compilation will be based on swath mapping using multibeam sonar which has a spatial resolution of about 400 m at a typical ocean depth of 4 km (Mayer et al., 2018).

The Seabed 2030 project has made considerable progress over the past few years by increasing the multibeam coverage in public compilations from 11% (e.g., Tozer et al., 2019) to more than 20% today. Much of this data has been made available by the international community with nearly complete coverage of several exclusive economic zones as well as dense coverage of areas of high scientific interest. The remaining 80% of the seafloor has depth predicted from a combination of spatially dense satellite altimeter gravity measurements and sparse soundings to provide the large-scale shape of the ocean basins as well as to calibrate the local ratio of bathymetry-to-gravity (e.g., Smith & Sandwell, 1994). The spatial resolution of these predicted depths is limited to approximately the mean ocean depth because of the upward continuation smoothing effects from Newton's law of gravity. The best satellite gravity models available today can only resolve  $\frac{1}{2}$  wavelength of 6 km when the regional depth is 4 km (Tozer et al., 2019). Thus, the resolution of gravity-predicted depth is more than 10 times worse than the Seabed 2030 objective.

There are many remote ocean areas in the southern hemisphere that will probably not be completely mapped at 400 m resolution during this decade and well beyond (e.g., Figure 1). This study is focused on the development of SYNthetic BATHymetry (SYNBATH) to fill the gaps. The synthetic bathymetry has the geostatistical properties of real seafloor bathymetry but it is not as accurate as ship soundings. While the synthetic data will be replaced with real soundings as they become available in the future, in the interim such realistic realizations can provide key inputs for a number of important scientific applications. We will discuss such applications, where this synthetic bathymetry is appropriate and valuable, and also discuss uses of synthetic bathymetry that could prove problematic and result in a false impression that Seabed 2030 objectives have been achieved.

There are two types of seafloor features that are not well resolved by satellite gravity; abyssal hills and small seamounts (<2.5 km tall). As described more completely in the next section, one can generate synthetic abyssal hills by combining the measured statistical properties of mapped abyssal hills with regional geology including fossil spreading rate/orientation, rms height from satellite gravity, and sediment thickness (Goff, 2010; Goff, 2020; Goff & Arbic, 2010). At scales greater than about 6 km  $\frac{1}{2}$  wavelength, the location or “phase” of the synthetic hills matches the actual location based on gravity predicted depth. At shorter scales, the synthetic hills have the correct power spectral roll-off and orientation but have random locations completely uncorrelated with the actual abyssal hills. For studies in physical oceanography, creating hills with the correct height, spectral slope, and orientation is more important than hills having the correct location or phase (Scott et al., 2011; Timko et al., 2017) although phase information will be needed for fully resolved models.

The second type of unresolved seafloor feature are seamounts less than about 2.5 km tall (Kim & Wessel, 2011, 2015; Menard, 1964; Staudigel et al., 2010). Because of significant improvements in the accuracy and resolution of the satellite gravity since the Kim and Wessel (2011) study, it is now possible to detect seamounts taller than about 800 m (Gevorgian et al., 2021) and their location can be determined to an accuracy of better than 1 km. However, the width of the gravity bump is much greater than the actual width of the seamount. Therefore, the seamount predicted from gravity will underestimate the seamount height and overestimate its base dimension. This results in a seamount flank slope that may be 10 times smaller than the actual slope (Becker & Sandwell, 2008). As in the case of abyssal hills, the magnitude of the slope of the seamount influences the paths of currents as well as the generation of eddies and internal waves. The studies by Smith (1988) and Gevorgian et al. (2021) have used depth soundings to characterize the shapes of smaller seamounts. In this study, we use the amplitude of the vertical gravity gradient (VGG) to estimate the mass of the seamount and then use their characteristic shape to replace the smooth predicted seamount with a Gaussian seamount having a more realistic shape.

## 2. Modeling Abyssal Hills

We use the model of Goff and Jordan (1988; 1989) to generate synthetic abyssal hills; the power spectrum of the topography has the following functional form

$$P(k_x, k_y) = \frac{\pi h_{\text{rms}}^2}{vk_n k_s} \left[ \frac{k_h^2}{k_s^2} \cos^2(\theta - \theta_s) + \frac{k_h^2}{k_n^2} \sin^2(\theta - \theta_s) \right]^{-(v+1)} \quad (1)$$

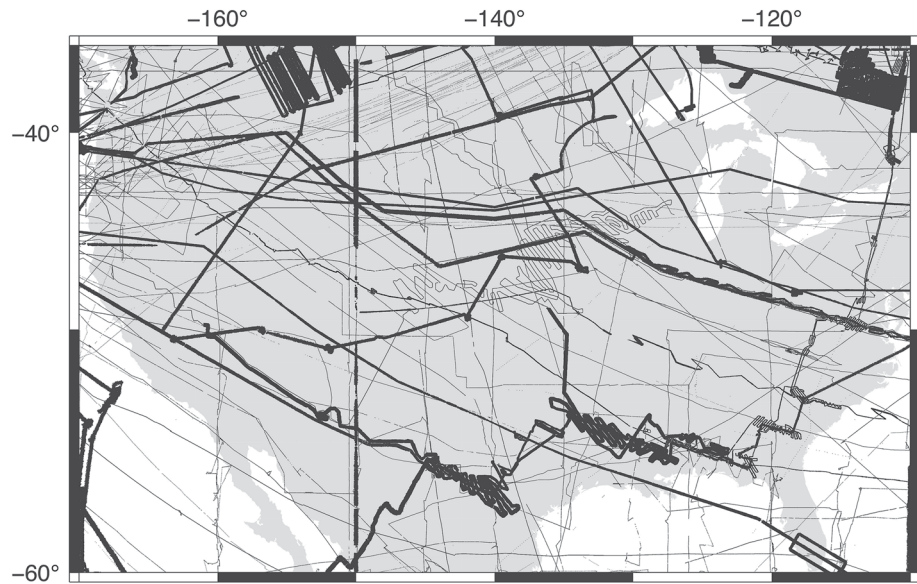


**Figure 1.** Available ship soundings including single-beam data (thin lines) and multibeam data (thick lines) in a remote region of the South Pacific based on the GEBCO 2021 bathymetry (GEBCO., 2020) grid superimposed on a map of North America for scale. There are many areas on this map that are more than 100 km from a depth sounding. Moreover, removal of the lower resolution single beam soundings would dramatically reduce the spatial coverage leaving many gaps greater than 400 km.

where  $(k_x, k_y)$  is the 2-D wavenumber,  $k_h = (k_x^2 + k_y^2)^{1/2}$  is the magnitude of the 2-D wavenumber,  $h_{\text{rms}}$  is the rms of the abyssal hill height,  $(k_s, k_n)$  are the characteristic wavenumbers for the abyssal hills in the strike and normal directions, respectively,  $\theta_s$  is the azimuth of the strike of the abyssal hills and  $v$  is the Hurst number ( $\sim 0.9$ ) that determines the rate of spectral roll-off. The five parameters ( $h_{\text{rms}}, k_s, k_n, \theta_s, v$ ) vary geographically depending on the geological setting at the time of the formation of the abyssal hills (Goff, 2020). In addition, as the plate ages, sediments can partially or fully cover the hills which reduces their visible height.

The rms height  $h_{\text{rms}}$  of the hills is taken from the most recent analysis (Goff, 2020) of the altimeter-derived gravity anomaly (Sandwell and Smith, 2019). RMS height was reduced in sediment-covered areas by a factor of 0.1 times the sediment thickness (Straume et al., 2019). The characteristic wavenumbers ( $k_s, k_n$ ) and Hurst number  $v$  were taken from the analysis of Goff (2010) and the orientation of the abyssal hills  $\theta_s$  is from the recent global age compilation of Seton et al. (2020).

To replace the predicted bathymetry with more realistic abyssal fabric, we first prepare the five global parameter grids ( $\pm 74^\circ$  latitude) to have consistent spatial coverage. This was done by extending the grids of  $(k_s, k_n, \theta_s, v)$  and then tapering the rms height grid  $h_{\text{rms}}$  to go smoothly to zero on its perimeter. As in previous studies (e.g., Goff & Arbic, 2010), we populate a 30 arcsecond global grid with uniform random cell values. A 2-D spatial filter is calculated from the inverse transform of the spectral model in Equation (1) at each cell location and convolved with the random grid; a new filter is computed at each grid cell to accommodate the spatial variations in the five parameters. This operation is equivalent to inverse Fourier transformation of the product of the amplitude spectrum with a random phase spectrum. However, though computationally far more efficient, this alternative does not allow for the imposition of the statistical heterogeneity that is critical for our purposes. The resulting synthetic bathymetry (e.g., Figure 2) is added to a previous iteration of global depth to make a new synthetic bathymetry data set. We then perturb the global predicted bathymetry model to exactly match these synthetic data using a standard remove/grid/restore approach (e.g., Sjöberg, 2005). A spline in tension gridded is used (Smith & Wessel, 1990). This becomes an updated predicted depth that is used in a second remove/grid/restore using the real sounding data. The final result exactly matches the real soundings where they exist and blends smoothly into the updated predicted depth in the data voids. The fully sedimented areas and areas with no abyssal hill predictions have depth based entirely on sparse soundings and the gravity prediction.

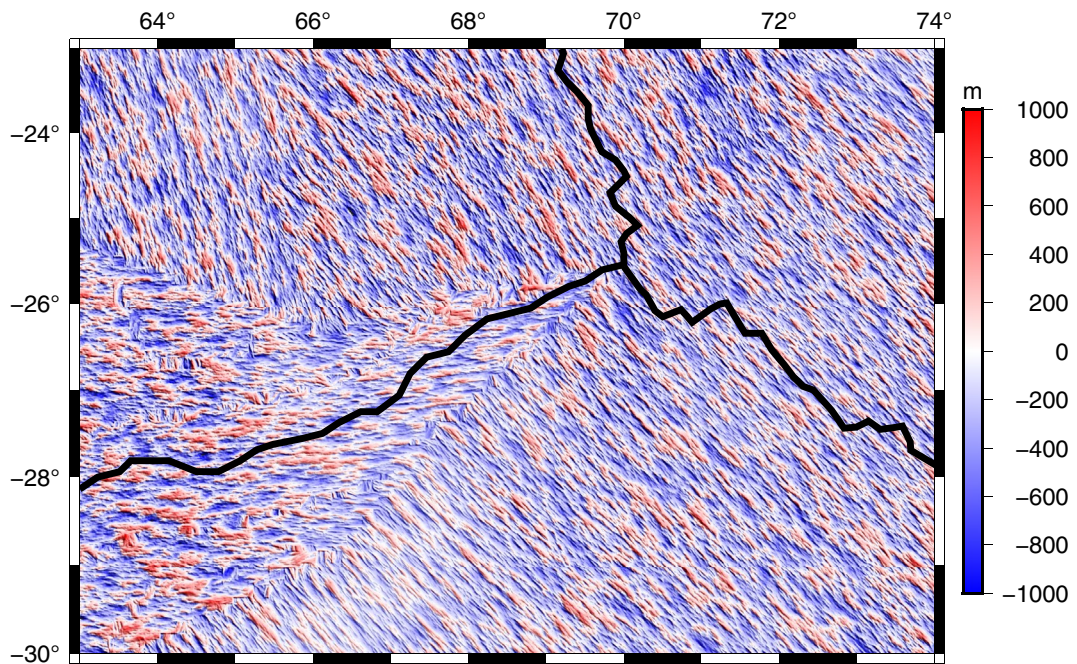


**Figure 2.** Example of synthetic abyssal hills around the Indian Ocean Triple Junction illustrate their variation with spreading direction and rate.

### 3. Mapping Seamounts

Although multibeam sonar is best suited for mapping smaller seamounts, satellite altimetry can be used to find larger seamounts ( $>700$  m) through disturbances in Earth's gravity field. These perturbations are due to the difference in density between basalt and seawater. There are four main errors and uncertainties that arise from satellite altimetry: upward continuation, measurement noise, seafloor roughness, and sediment cover (Wessel et al., 2010). The first global seamount maps (8,556 seamounts) were created from widely spaced Seasat altimeter profiles (Craig & Sandwell, 1988). Since the Seasat mission, there have been a number of altimeter missions that have greatly improved the accuracy and coverage of the gravity field (Wessel, 2001, 14,639 seamounts). This has enabled the construction of the vertical gravity gradient (VGG) which is a spatial derivative of the gravity field (e.g., Wessel, 1997). This spatial derivative amplifies short wavelengths and suppresses long wavelengths so it is a valuable tool for locating smaller features on the ocean floor (Kim & Wessel, 2011, 2015). However, the spatial derivative also amplifies short wavelength noise which limits seamount detectability. The recently released VGG has significantly lower noise levels because of new altimeter data from CryoSat-2, SARAL/AltiKa, Jason-1/2, and the Sentinel-3a/b missions (Sandwell et al., 2014, 2021). After comparing the old and new VGG, it was found that the signal-to-noise ratio has increased by at least a factor of 2, indicating that multiple altimetry sources can improve gravity data and help find unmapped features on the ocean floor.

Gevorgian et al. (2021) have used the latest version of the VGG model (Sandwell et al., 2021) to update the global seamount catalog of Kim and Wessel (2011, 2015). The original KW catalog had 24,643 seamount identifications. The new analysis was performed in four steps using the display and digitization features in Google Earth: (a) The VGG was displayed as a gray-scale image with black-to-white saturation set at  $-53$  to  $+38$  Eotvos units. (b) Known tectonic features (Matthews et al., 2011) were plotted as lines. (c) The KW15 catalog was also plotted as points. (d) Gevorgian et al. (2021) visually identified circular anomalies in the VGG in the deep ocean ( $>\sim 500$  m) away from known and well-mapped tectonic features. The lower noise level in the latest VGG grid enabled the identification of circular anomalies as small as 5 Eotvos which is about  $\frac{1}{2}$  the threshold of the KW15 analysis. Gevorgian et al. (2021) found 10,796 previously unidentified seamounts and also determined that 513 seamounts in the KW15 catalog were mis-identifications. The revised KW catalog has 24,129 seamounts so the total seamount count is 34,925. Figure 3 shows a region on the eastern flank of the East Pacific Rise where there

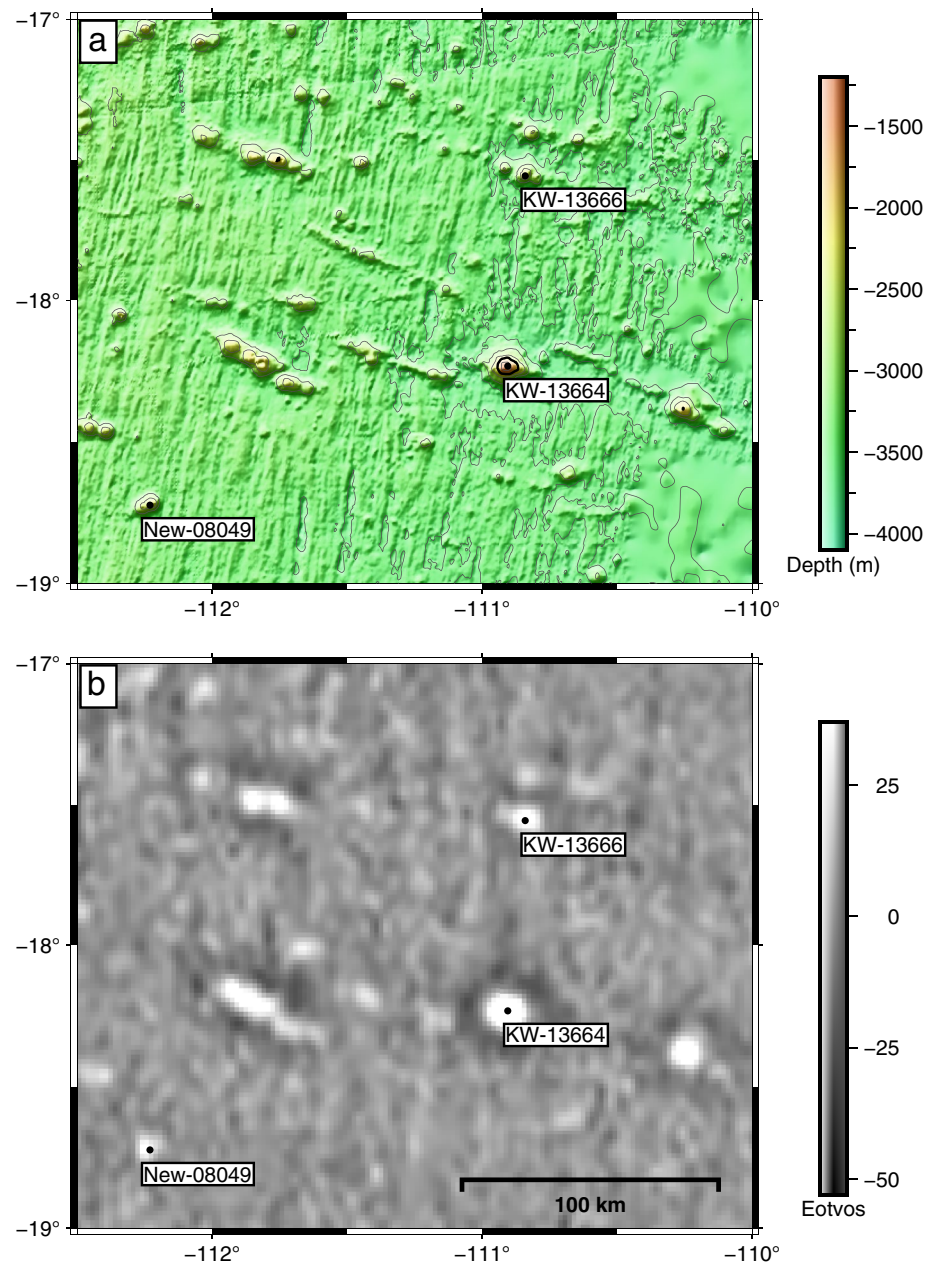


**Figure 3.** (a) Bathymetry on the eastern side of the East Pacific Rise (EPR) where three seamounts have been mapped by multibeam sonar. The two labeled KW are from the Kim and Wessel (2011) catalog while the seamount labeled New-08049 is from Gevorgian et al. (2021). (b) VGG in the same area showing three seamounts that are relatively circular.

is complete multibeam coverage. The VGG image shows numerous circular anomalies associated with small seamounts. We use these to develop a method of estimating seamount height and radius from the VGG anomaly.

#### 4. Modeling Seamounts

Previous studies have found that small seamounts are typically circular in planform and have a fixed height to base ratio largely independent of height (Smith & Jordan, 1988; Wessel, 2001). Smith (1988) studied bathymetry profiles across 85 seamounts and found they could be fit by a flattened cone having a height to base radius ratio of  $\sim 0.21$  and a flattening of 0.15. More recently, Gevorgian et al. (2021) studied 739 seamounts having at least

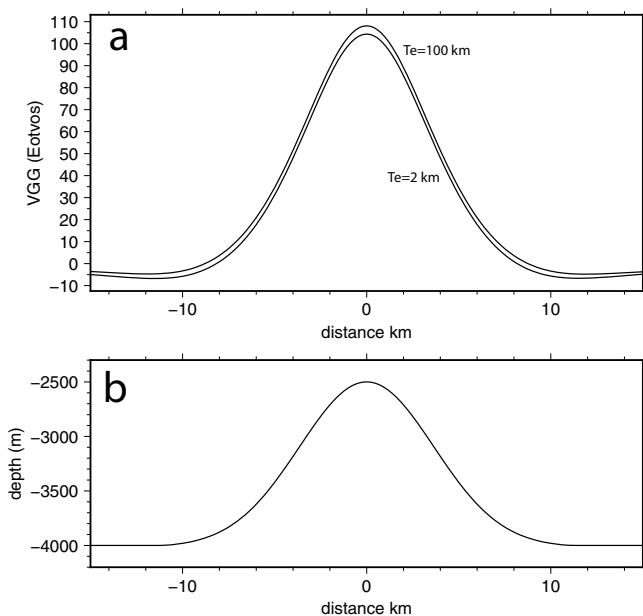


**Figure 4.** Vertical gravity gradient (VGG—*a*) computed from a Gaussian seamount (*b*) that is 1,500 m tall, has a  $\sigma = 2.4h_o$ . The two VGG curves, which are very similar, correspond to well-compensated topography ( $T_e = 2$  km) and uncompensated topography ( $T_e = 100$  km).

50% coverage of the seamount and complete coverage of the summit area. Using these well-surveyed seamounts they found, on average, they are best fit by a Gaussian function

$$h(r) = h_o e^{-\frac{r^2}{2\sigma^2}} \quad (2)$$

where  $h_o$  is the seamount height,  $r$  is the radius from the center of the seamount, and  $\sigma$  is the characteristic width of the seamount. Their analysis found a high correlation between seamount radius and slope such that  $\sigma = 2.4h_o$ . This corresponds to a maximum seamount slope of 0.25 independent of seamount height. Here we use this model, along with the observed VGG, to estimate the shape of each seamount. There are several parameters that go into this gravity modeling including mean ocean depth surrounding the seamount  $d_o$ , seamount density relative to seawater  $\Delta\rho$ , crustal thickness, elastic thickness, mantle density, and seamount height  $h_o$ . We show next that for seamounts  $<\sim 2$  km in height, the VGG is insensitive to the elastic thickness so we can assume the seamounts are uncompensated. In this case the mean crustal thickness and mantle density are not needed.

This insensitivity to elastic thickness is easily verified using the *grdseamount* and *gravfft* modules in generic mapping tools (GMT) (Wessel et al., 2019). A typical seamount, shown in Figure 4, has a height of 1,500 m, a  $\sigma = 2.4h_o$ , a density of 2,700 kg m<sup>-3</sup>, and a base depth of 4,000 m. To assess the effects of elastic thickness, we computed the VGG, including three nonlinear terms in the Parker (1973) expansion. For an elastic thickness  $T_e$  of 2 km as well as 100 km (uncompensated), the two VGG models have almost equal signatures so we can assume small seamounts are uncompensated as in Watts et al. (2006).

Based on this calculation the remaining free parameters are seamount height, seamount density, and base depth. The base depth is calculated from the median depth in a 90 km by 90 km area surrounding the seamount to be modeled.

To further test the validity of this simple model for a small seamount, we analyzed topography and VGG for three seamounts in an area of the southern East Pacific Rise where there is complete multibeam coverage (Figure 3). Two of the seamounts are from the Kim and Wessel (2011) compilation while the third is recently identified in the VGG (Gevorgian et al., 2021). The basic characteristics of the seamounts are provided in Table 1.

Using these well-surveyed seamounts, we can perform forward modeling to establish the density that provides the best fit. From the observed topography we calculate the VGG and compare with the observations. An additional low-pass filter, with a wavelength of 16 km, was applied to the model VGG to match the low-pass filtering that was used to construct the VGG data (Sandwell et al., 2021). Table 2 shows the median absolute deviation (L1-norm) as a function of seamount/crustal density for each of the three seamounts. We find that the misfit is not very sensitive to the density. A much more extensive study by Watts et al. (2006) using 9,752 seamounts shows the best density is 2,800 kg m<sup>-3</sup>. This value is consistent with our results from modeling just three small seamounts.

**Table 1**  
*Characteristics of Modeled Seamounts*

Label	Lon.	Lat.	Base depth(m)	Seamount height (m)	Gravity (mGal)	VGG (Eotvos)
KW-13664	-110.90	-18.23	3461.5	2140	53.4	143.7
KW-13666	-110.84	-17.54	3409.5	1343.5	18.5	50.8
New-08049	-112.23	-18.71	3255.5	1209.5	12.9	44.7

**Table 2**  
*Misfit (L1-Norm) Versus Seamount Density in Eotvos*

	2,650 kg m <sup>-3</sup>	2,700	2,750	2,800	2,850	2,900	No model
KW-13664	4.51	4.34	4.33	4.43	4.50	4.56	10.49
KW-13666	4.35	4.28	4.19	4.19	4.20	4.21	8.74
New-08049	4.49	4.51	4.53	4.54	4.54	4.45	5.51

An example of the fit of the model to the largest of the three seamounts is shown in Figure 5. The model based on topography with a density of 2,800 kg m<sup>-3</sup> provides an excellent fit to the VGG data. As a final check we generated VGG models using a Gaussian approximation to the actual seamount topography for large and small seamounts in the region. These results, shown in Figures 5 and 6, demonstrate that the VGG from a Gaussian seamount is a good match to the VGG from the actual seamount topography. The important parameter is the seamount height. Because most seamounts are uncharted we will use this approach, with a Gaussian shaped seamount, to generate synthetic seamounts in unmapped areas.

Based on this analysis, we estimated heights for 34,925 seamounts in the updated catalog basically using the method of Wessel (2001). This was done by extracting a 90 km by 90 km grid of VGG and SRTM15 (V2.3) depth data centered on each seamount. The base depth was computed from the median depth of this larger 90 km grid and a Gaussian seamount (Equation 2) was superimposed on this base depth using  $\sigma = 2.4h_o$  a density of 2,800 kg m<sup>-3</sup>. The VGG model, generated using *gravfft* in GMT, was low-pass Gaussian filtered at 16 km wavelength to match the low-pass filter applied to the VGG data. Finally, the L1 norm difference between the model and data VGG was computed for a smaller 33 by 33 km area centered on the seamount. This modeling was repeated for seamount heights ranging from 700 to 2,600 m in steps of 100 m. The model with the lowest misfit was selected as the height. A histogram of the number of seamounts versus their estimated height is shown in Figure 7(top). A histogram of seamounts versus the L1 norm of the misfit is shown in Figure 7(bottom). For all seamounts, the number increases with decreasing seamount height until 1,300 m when the number decreases at smaller heights. Our results show that the KW analysis, using noisier VGG data, captured most seamounts taller than about 1,500 m. The new analysis found many more seamounts with heights between 1,100 and 1,500 m. Most of the VGG models have misfits between 5 and ~20 Eotvos. The new seamounts are generally smaller and have lower L1-misfit. For the remainder of this study, we exclude all seamounts with heights greater than 2,500 m and less than 800 m since they are at the ends of the histogram. We also reduce the height of any seamount having a depth shallower than -100 m to force the model summit depth of -100 m. In other words we do not want to create any

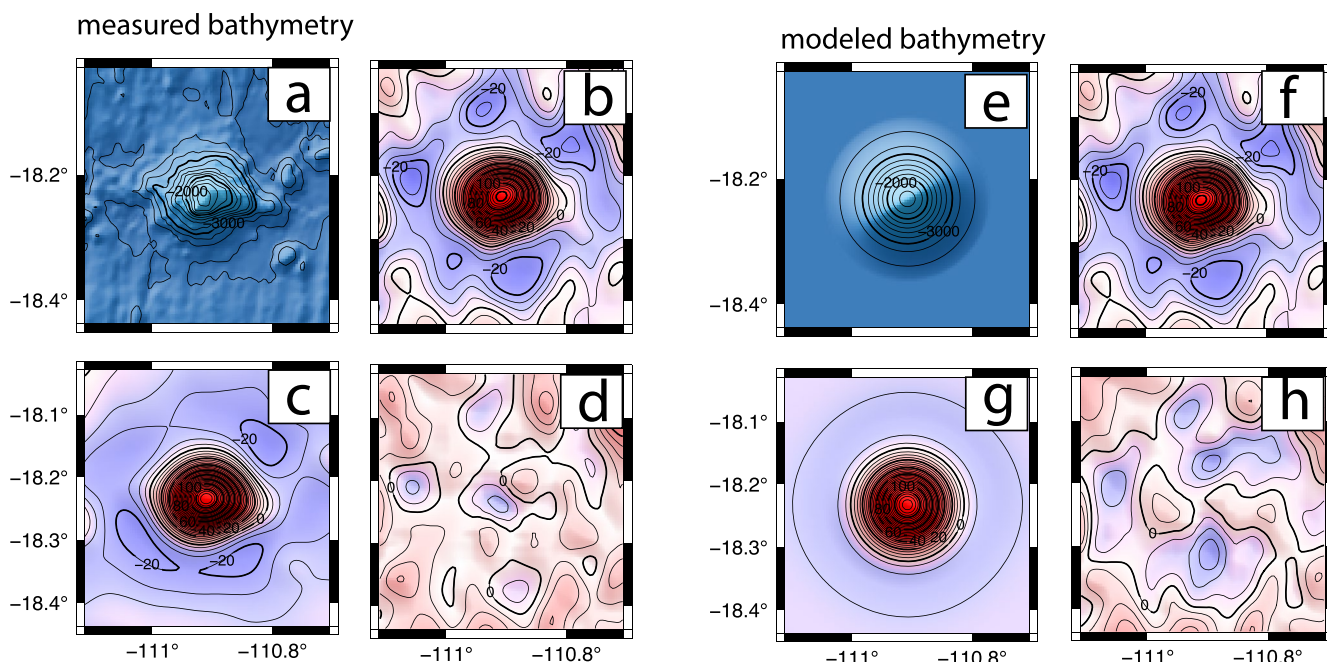


**Figure 5.** (a) Bathymetry of the largest of the three seamounts, KW-13664 (200 m contours). (b), (f) Measured VGG for seamount (5 Eotvos contours). (c) Model VGG using a density of 2,800 kg m<sup>-3</sup>. (d) Difference between observed VGG and model VGG (L1-norm, 4.43 Eotvos, 5 Eotvos contours). (e) Model bathymetry using a Gaussian seamount (200 m contours). (g) Model VGG for Gaussian model bathymetry. (h) Difference between observed VGG and Gaussian model VGG (L1 7.04 Eotvos, 5 Eotvos contours).

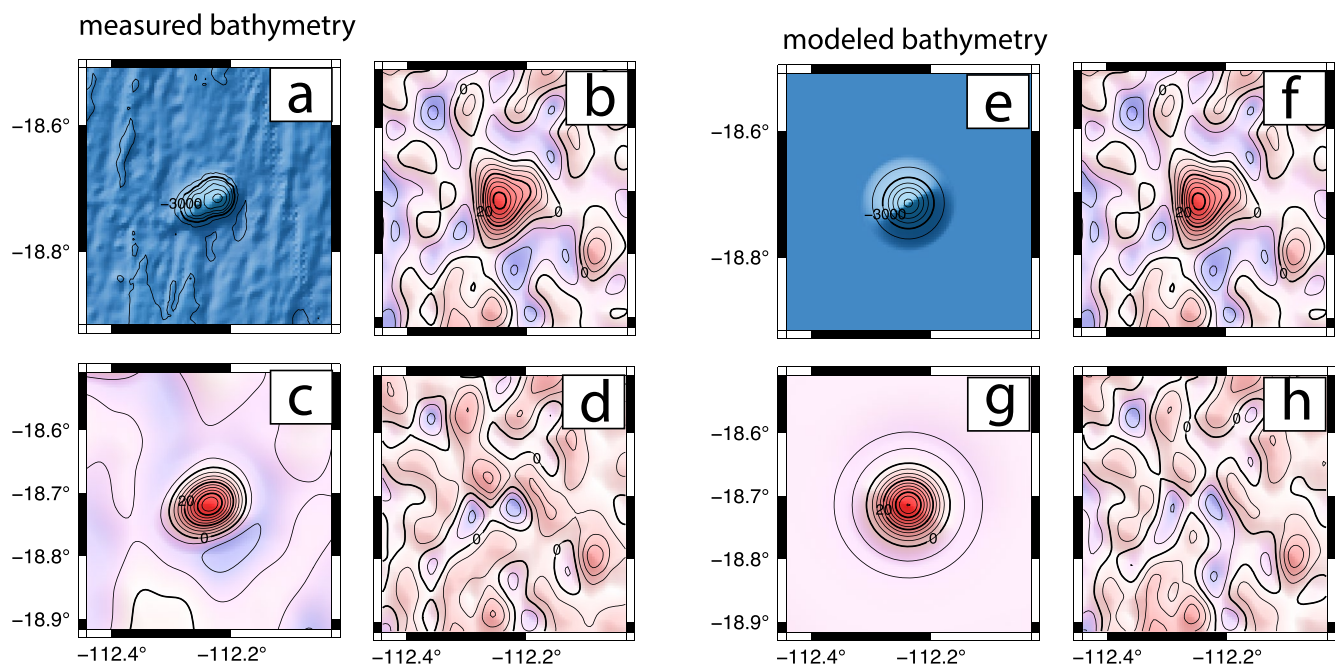


**Figure 6.** (a) Bathymetry of the smallest of the three seamounts, New-08049 (200 m contours). (b + f) Measured VGG for seamount (5 Eotvos contours). (c) Model VGG using a density of  $2,800 \text{ kg m}^{-3}$ . (d) Difference between observed VGG and model VGG (L1 4.54 Eotvos, 5 Eotvos contours). (e) Model bathymetry using a Gaussian seamount. (g) Model VGG for Gaussian bathymetry (200 m contours). (h) Difference between observed VGG and conical model VGG (L1 5.13 Eotvos, 5 Eotvos contours).

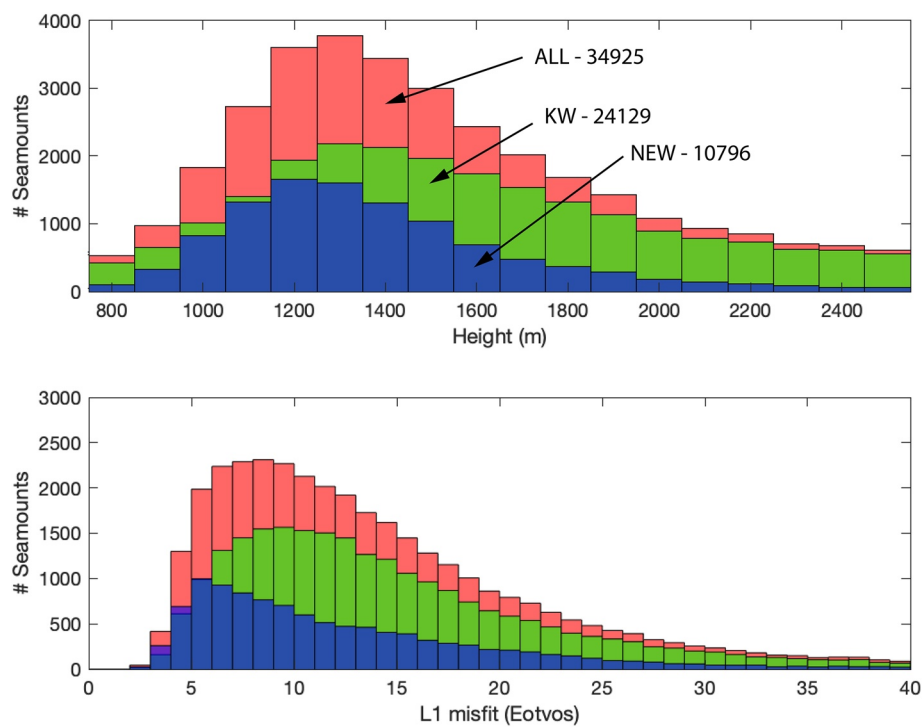


**Figure 7.** (Top) Histogram of the seamount height based on our analysis of all seamounts (red), KW seamounts (green), and new seamounts (blue). (Bottom) Histogram L1 misfit of model VGG to each seamount.

false islands or atolls although these cases may be interesting places to survey with multibeam. This results in 31,602 modeled seamounts.

We investigate how many of these seamounts are constrained by depth soundings by using the SRTM15 V2.3 source identification grid (SID) to locate all the seamounts having at least one sounding within 3 km of the center of the seamount. This resulted in 11,879 seamounts that are at least partly constrained by a real depth sounding and 19,723 seamounts that are completely uncharted.

## 5. Results

Prior to filling the gaps with synthetic bathymetry, we assembled new sounding data not available for the Tozer et al. (2019) study. The latest V2.3 of the SRTM15+ grid includes 905 new multibeam sonar cruises that are archived at the National Center for Environmental Information (<https://www.ngdc.noaa.gov/mgg/bathymetry/multibeam.html>). These were processed with MB-System (Caress & Chayes, 2008) to remove outer beams and flatten the rails of the innermost beams, and subsequently used to update the 15-arcsecond grid. We performed three iterations of visual editing of bad soundings (~700 edits) to prepare the grid as the base layer for the GEB-CO 2022 global grid. In addition we obtained nine large composite grids from IFREMER that greatly improved the bathymetry coverage of the Gulf of Aden (Hebert et al., 2001), the Lesser Antilles volcanic arc (Talbot & Loubrieu, 2020), French Guiana margin (Loubrieu, 2019a), the Rodrigues triple junction (Mendel et al., 2000), the Kerguelen plateau (Loubrieu, 2019b), Reunion island (Sisavath et al., 2011), Saint-Paul and Amsterdam Islands (Loubrieu et al., 2020), the Southwest Indian ridge (Sauter & Mendel, 2000), and the North Fiji basin (Ruellan, 2001).

Gaps in the SRTM15+ grid were filled with synthetic bathymetry to create SYNthetic BATHymetry (SYNBATH V1.2). An example of the enhancement related to just abyssal hills is shown in Figure 8. The upper plot shows the standard SRTM15+ grid with the combination of single- and multibeam bathymetry and smooth gravity-predicted depths filling the gaps. The Indian Ocean triple junction at 70° longitude and –25.7° latitude is the intersection of the Central Indian ridge (CIR) to the north, the Southeast Indian ridge (SEIR), and the Southwest Indian ridge (SWIR). The flanks of each ridge have ridge-parallel abyssal hills as seen in the available multibeam bathymetry. The slower spreading SWIR has left a V-shaped scar on the seafloor where there is a nearly 90° change in the orientation of the abyssal hills reflecting the change in age gradient (e.g., Seton et al., 2020). The center plot shows the SYNBATH bathymetry which is identical to the SRTM15+ bathymetry where there are real ship soundings and has synthetic abyssal hills in the gaps. The boundaries between the actual and synthetic bathymetry are difficult to observe. One would expect a sharp change in the “phase” of the abyssal hills across these boundaries. However, a part of the synthetic abyssal fabric contains a correct-phase pattern that is derived from the gravity prediction. Figure 8c shows the difference between the SYNBATH and SRTM15+ bathymetry grids. The difference is zero at grid cells constrained by ship data and matches the synthetic abyssal hills (Figure 2) in the gaps.

An example of the enhancement primarily related to small seamounts is shown in Figure 9 for a poorly charted region just south of the Galapagos spreading ridge. The smaller predicted seamounts, having no bathymetry soundings, are short and wide (Figure 9a). The sharpened seamounts are tall and narrow following the shape of the Gaussian model  $\sigma = 2.4h_o$  (Figure 9b). The difference between these two models (Figure 9c) shows the combined effects of added abyssal fabric and sharpened seamounts. In areas where there are actual multibeam depth soundings, the two models agree.

Since there are many steps in constructing this SYNBATH bathymetry at 15 arcseconds we provide a brief overview. There is a common polishing technique used each time a new data layer is added so we first describe that remove/grid/restore approach as follows: (a) assemble some new data e.g., real soundings or synthetic hills or seamounts; (b) remove the previous model from each new data point; (c) identify spatial gaps (>20 km from a new data point) and add zero-valued data points at these locations; (d) use the GMT surface module with a tension of 0.6 and a convergence limit of 1 m and up to 200 iterations; (e) add the previous model so the result exactly fits the new data. Given this common polishing approach the overall construction method is:

1. Use the gravity prediction method described in Smith and Sandwell (1994) and updated in Tozer et al. (2019) to make a global 1-min bathymetry
2. Polish that bathymetry using actual soundings

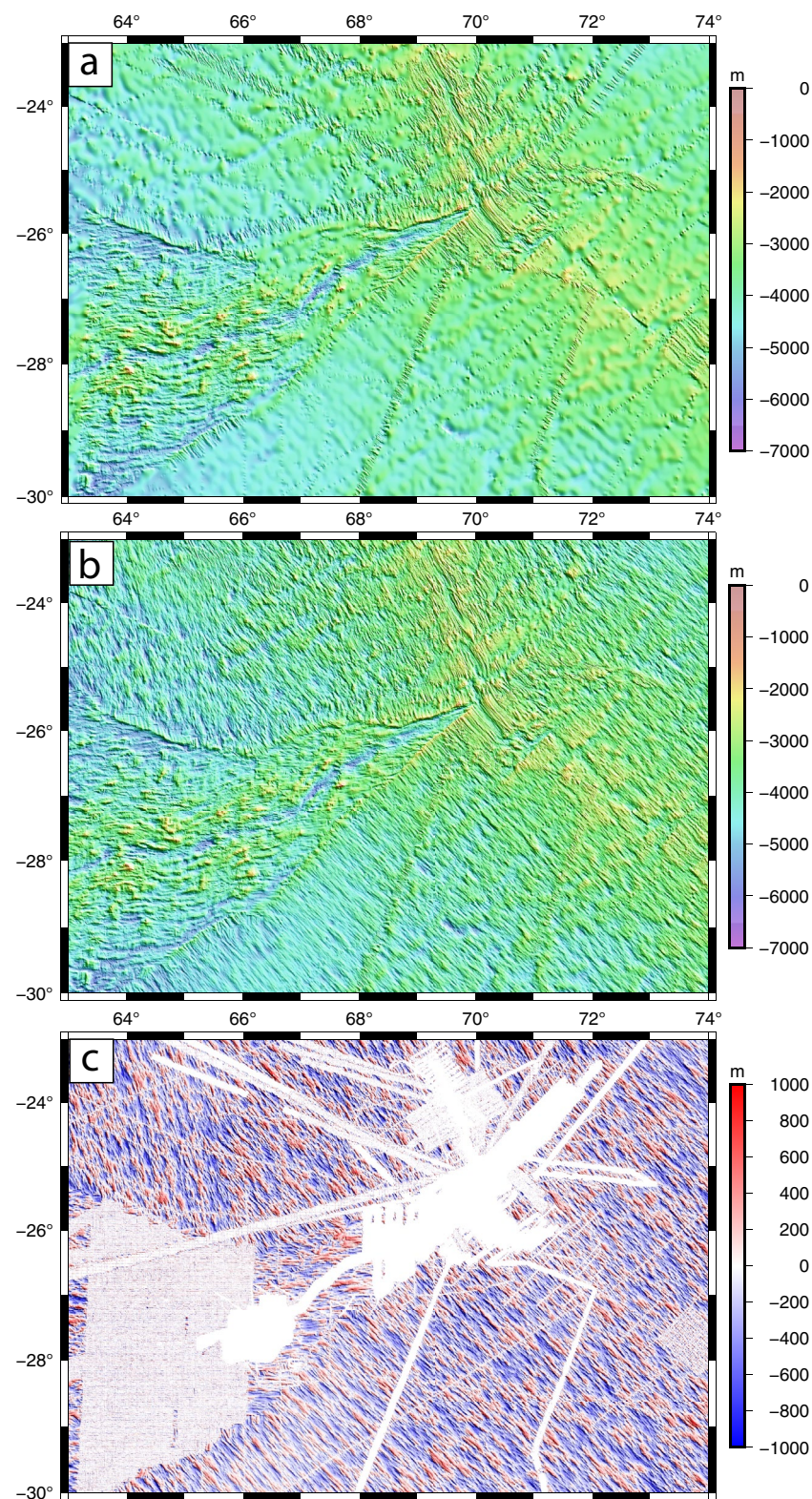


**Figure 8.** Bathymetry of Indian Ocean Triple Junction. (a) Based on multi- and single-beam soundings and gravity-predicted bathymetry to fill the gaps. (b) Based on multi- and single-beam soundings and synthetic abyssal hills superimposed on gravity-predicted bathymetry to fill the gaps. (c) Difference shows that the two methods are identical where measured soundings are available and have synthetic abyssal hills in other areas.

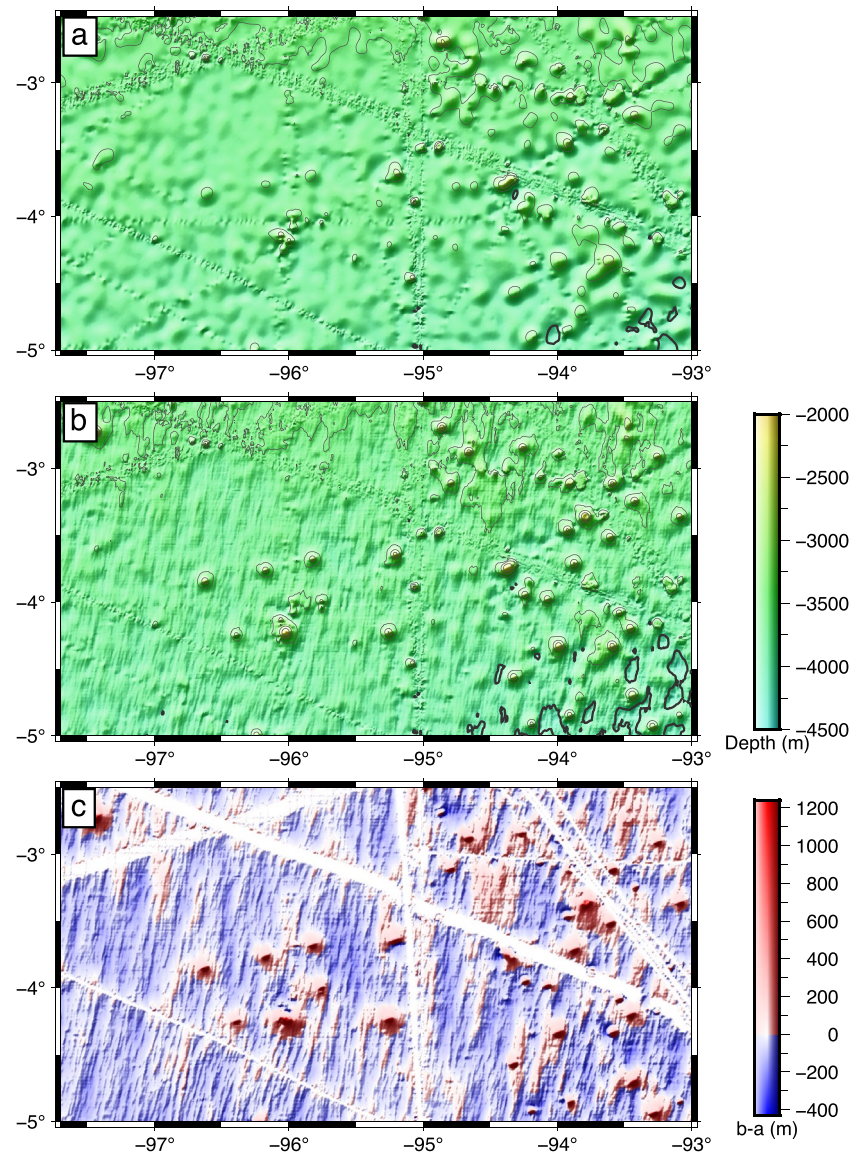


**Figure 9.** Bathymetry of an area south of the Galapagos spreading ridge. (a) Based on multi- and single-beam soundings and gravity-predicted bathymetry to fill the gaps. (b) Based on multi- and single-beam soundings, synthetic abyssal hills and sharpened seamounts superimposed on gravity-predicted bathymetry to fill the gaps. (c) Difference shows that the two methods are identical where measured soundings are available and have synthetic abyssal hills in other areas. Uncertainty of the Synthetic Bathymetry.

3. Use the 1-min base depth to generate synthetic abyssal hill data and synthetic seamount data. So the model from step (2) provides the base depth for both the hills and seamounts. Also note the synthetic seamount data extend only  $1.5\sigma$  from the seamount center. This promotes better blending of the synthetic seamounts into the regional bathymetry while retaining the data having maximum slope which occur at  $1.0\sigma$
4. Create a 15-arcsecond grid following the methods in Tozer et al. (2019)
5. Polish the step (4) grid with synthetic abyssal hills
6. Polish the step (5) grid with synthetic seamounts
7. Polish the step (6) grid with all the real soundings
8. Combine the land topography data with the grid from (7)

This is a rather complex recipe. However, it is designed to inherit the long-wavelength shape of the ocean basins from original depth soundings. The satellite-derived gravity is used next to update the bathymetry in the

160–16 km wavelength band. Short wavelengths between 16 and 1 km are updated with synthetic abyssal hills. This is followed by an update using the Gaussian seamounts which, as in the real world, overprint the abyssal hills. Finally, the grid is polished using real depth soundings.

Two approaches were used to assess the accuracy of the synthetic bathymetry with respect to the gravity-predicted depths. First, we compared the accuracy of seamount summit depths for the 739 well-surveyed seamounts from the Gevorgian et al. (2021) study. When constructing the global predicted depths we first construct a global bathymetry grid using only the satellite-derived gravity as described in the Tozer et al. (2019) study. Available depth soundings are used to calibrate the topography-to-gravity ratio in the 160–18 km wavelength band averaged over an area about 320 km in diameter. The predicted bathymetry in areas of complete multibeam coverage has the same characteristics as the bathymetry in the gaps so the actual multibeam soundings can be used to assess the accuracy of the predicted depth. Figure 10 (left) shows a comparison of the predicted and measured summit depth of the 739 well-surveyed seamounts. As discussed above, the predicted summit depths are almost always less than the actual depth. This analysis shows that the median difference is  $-555$  m and the median absolute deviation (L1) is 264 m. The same analysis for the sharpened seamounts based on VGG modeling (Figure 10, right) has a much smaller median difference of 55 m and a slightly larger median absolute deviation of 272 m. This analysis shows that the sharpened seamounts have more accurate summit depths although the Gaussian shape model does not recover the details of the actual seamount shape.

For the second analysis, we have obtained a recent multibeam sonar survey in the North Atlantic collected from the RV Maria S. Merian (GEOMAR, Devey et al., 2020; Wölfl and Devey, 2020). We selected a subset of these data in a region where there were no previous soundings (Figures 11b) and compared the measured depth with both the gravity-predicted depth (Figures 11a) and the predicted depth augmented with synthetic abyssal hill fabric (Figures 11c). As expected the gravity-predicted depth is much smoother than the actual depth with a median difference of  $-66$  m and a median absolute deviation (L1) of 241 m. The synthetic bathymetry has abyssal hills that look similar to the measured abyssal hills but the random location of the synthetic hills does not match the actual measured location resulting in a median depth difference of 8 m and a L1 of 323 m. Therefore, the addition of the synthetic abyssal hills has increased the error in the depth by a factor of 1.34. This highlights that the synthetic bathymetry should not be used for any application where knowing the depth of specific points is important but, as discussed above, the synthetic bathymetry has small-scale roughness and slope characteristics that better match the actual bathymetry.

This synthetic bathymetry has some appropriate uses as well as some uses that are inappropriate (Table 3) so it will be important to educate the users on how to use the product. A significant danger is that the general public could examine the synthetic bathymetry using a graphical tool such as Google Earth and conclude that the seafloor has been completely mapped at  $\sim 500$  m resolution. Therefore, there must be an additional graphical layer, or style, to indicate what is real and what is synthetic.

The applications where this product is not useful are mainly aligned with GEBCO applications. These include seafloor geography and feature names. All of these synthetic features lie at base depths greater than  $\sim 1,000$  m so they are irrelevant for any kind of navigation except the 149 seamounts extending to within 200 m of the sea surface; these need to be flagged with red dots and eventually surveyed ([https://www.star.nesdis.noaa.gov/star/documents/meetings/extReview/presentations/5CommTrans/CT2\\_WSmith.ppt](https://www.star.nesdis.noaa.gov/star/documents/meetings/extReview/presentations/5CommTrans/CT2_WSmith.ppt)). This product is not useful for establishing the boundaries of the outer continental shelves for the law of the sea. The product is not useful for any kind of detailed deployment of seafloor instrumentation although it can provide a regional sense of seafloor roughness at scales larger than 1 km. Since the synthetic bathymetry is confined to the deep ocean where sediments are thin it is not useful for any applications on the continental margins.

There are three applications where this product is marginally useful. (a) In terms of education and outreach it could provide misinformation that we are done mapping the deep oceans. However, like the early hand-drawn bathymetric maps from Heezen and Tharp (1959) and GEBCO (Hall, 2006), the realistic synthetic bathymetry could inspire students to better understand marine geology and plate tectonics. (b) The product could help with establishing a range of possible tsunami propagation models based on statistical realizations of abyssal fabric and seamounts (Sepulveda et al., 2020). (c) It could be useful for understanding habitats over unmapped, moderately large seamounts.

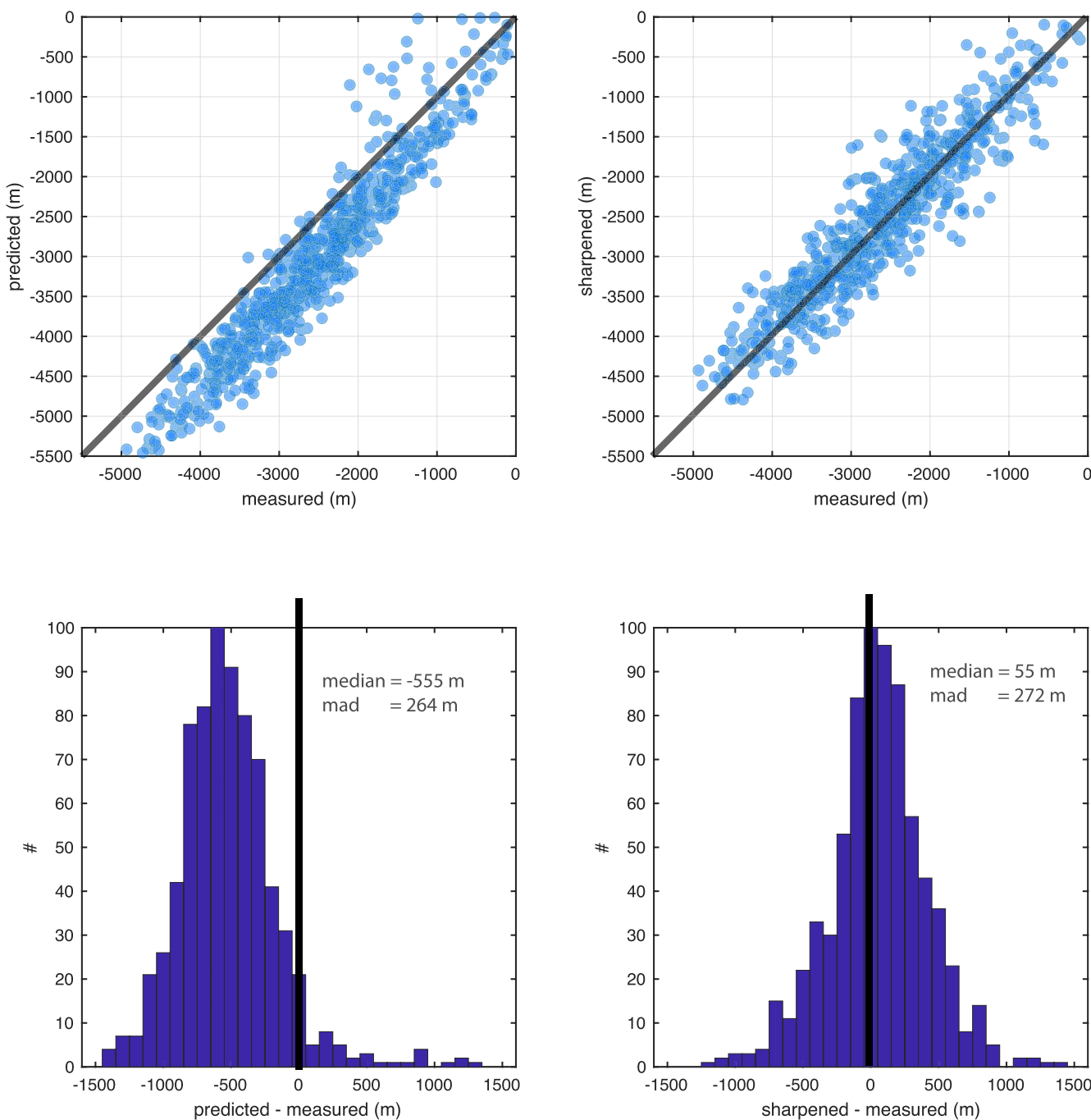


**Figure 10.** (Left) Gravity-predicted summit depth versus measured summit depth. The predicted summit depth is commonly 555 m deeper than the measured summit depth for these 739 well-charted seamounts. (Right) Summit depth for sharpened seamounts versus measured summit depth has 10 times smaller median difference of 55 m although the uncertainty is slightly larger (272 m).

The synthetic bathymetry is most useful for studies where a realistic seafloor roughness is needed. This includes models of ocean circulation (Adcroft et al., 2004; Chassignet et al., 2007) and internal wave generation, dissipation, and mixing driven by tidal and other low-frequency flows over the rough bottom (Egbert & Ray, 2003; Gille et al., 2000; Goff & Arbic, 2010; Jayne & St. Laurent, 2001; Polzin et al., 1997). In addition, rough seafloor affects the propagation of acoustic waves (e.g., Chin-Bing et al., 1994; Mackenzie, 1961). The product could be useful for plate tectonic studies since one can see where the abyssal hill fabric disagrees with nearby multibeam mapping which will provide data on how to revise tectonic models. Finally, the product could be useful for

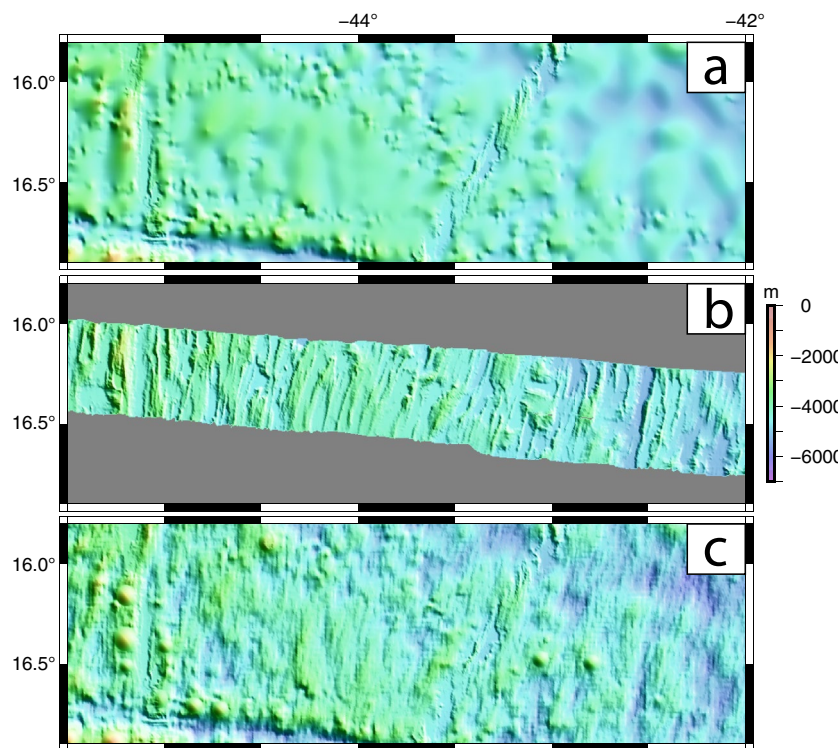


**Figure 11.** (a) Predicted depth based on gravity in the 160–18 km wavelength band is very smooth. (b) Measured seafloor depth from GEOMAR cruises. (c) Synthetic depth where the gravity-predicted depth has been augmented with synthetic abyssal hills as well as sharpened seamounts. Uses of Synthetic bathymetry.

planning shipboard surveys of seamounts and volcanic ridges as well as a tool for planning the optimal ship path for mapping rough seafloor.

## 6. Conclusions and Future Improvements

Our major conclusions are:

1. Bathymetry predicted from satellite altimeter-derived gravity cannot resolve the small-scale fabric of the deep ocean associated with abyssal hills and seamounts. There are many remote areas that will not be mapped by ship in this decade
2. We extend two methods to fill these gaps with higher resolution synthetic bathymetry using information on the tectonics, geology, and sediment distribution in the deep oceans
3. Synthetic abyssal hills are generated using an anisotropic statistical model based on high-resolution multibeam surveys in a variety of tectonic settings. The orientation of the hills uses the latest seafloor age maps
4. Small seamounts >700 m tall can be accurately located in satellite-altimeter-derived gravity but their shape cannot be resolved. We use ~800 well-surveyed small seamounts to calibrate the expected shapes of and create synthetic bathymetry for all seamounts in the 800–2,500 m height range
5. These two synthetic data sets are used to add a small-scale bathymetry component (1–16 km) to the global-predicted depth. This provides a new starting model for a remove/grid/restore re-gridding of available single and multibeam ship soundings

**Table 3**  
*Appropriate Applications of Synthetic Bathymetry*

Application	Yes	Maybe	No
Seafloor geography and feature names		X	
Navigation		X	
Law of the sea		X	
Fiber optic cable route planning		X	
Coastal tide model improvements		X	
Education and outreach	X		X
Tsunami propagation and hazard models	X		
Fisheries management		X	
Hydrodynamic tide models and tidal friction	X		
Ocean circulation models	X		
Tidal role in ocean mixing	X		
Plate tectonics	X		
Planning shipboard surveys	X		

6. We generate two global bathymetry/topography products at 15 arcseconds using identical ship soundings. The SRTM15+ product has gaps filled with smooth predicted bathymetry and serves as the base layer for the 15-arcsecond GEBCO grid. The SYNBATH product has gaps filled with synthetic bathymetry from abyssal hills and seamounts superimposed on the smooth predicted bathymetry
7. The SRTM15+ product is suitable for applications in seafloor geography, law of the sea, seafloor instrumentation and cables and highlighting the need to fill the gaps before 2030
8. The SYNBATH product is suitable for any application where an accurate seafloor roughness is needed such as modeling ocean currents and tidal friction and the generation and dissipation of internal waves

In the future, we plan to continue to improve the resolution of gravity-predicted depth as well as to work with GEBCO to assemble more multibeam sounding data. With these efforts we can roll-back the spectral and spatial contributions of the synthetic bathymetry. Ka-band altimeters such as SARAL/AltiKa and SWOT promise a dramatic improvement in marine gravity/bathymetry accuracy and resolution.

## Data Availability Statement

The global bathymetry grids and the characteristics of the 35,000 seamounts, and Google Earth overlays are all available at the ZENODO repository, <https://zenodo.org/deposit/5784502>, <https://doi.org/10.5281/zenodo.5784502>, in addition we keep a copy at our own open web site <https://topex.ucsd.edu/pub/>. The VGG grids and overlays are in the global\_grav\_1 min folder, the synthetic bathymetry and products are in the synbath folder, and the SRTM15+ bathymetry and products are in the srtm15\_plus folder. Figures and most calculations were performed using GMT (<https://www.generic-mapping-tools.org>) and MATLAB (<https://www.mathworks.com/products/matlab.html>). The authors also have all archived versions of our global grids in one location <https://topex.ucsd.edu/pub/archive/>.

## Acknowledgments

This work was supported by the Office of Naval Research (N00014-17-1-2866), NASA SWOT program (NNX16AH64G and 80NSSC20K1138) and the Nippon Foundation through the SeaBed2030 project. The Generic Mapping Tools (GMT) (Wessel et al., 2019) were extensively used in data processing. The views, opinions, and findings contained in the report are those of the authors and should not be construed as an official National Oceanic and Atmospheric Administration or U.S. Government position, policy, or decision.

## References

- Adercroft, A., Hill, C., Campin, J. M., Marshall, J., & Heimbach, P. (2004). September. Overview of the formulation and numerics of the MIT GCM. In *Proceedings of the ECMWF seminar series on Numerical Methods, Recent developments in numerical methods for atmosphere and ocean modelling* (pp. 139–149).
- Becker, J. J., & Sandwell, D. T. (2008). Global estimates of seafloor slope from single-beam ship soundings. *Journal of Geophysical Research: Oceans*, 113(C5). <https://doi.org/10.1029/2006jc003879>
- Caress, D. W., & Chayes, D. N. (2008). MB-System: Open source software for the processing and display of swath mapping sonar data. Internet: <http://www.mbari.org/data/mbsystem>
- Chassignet, E. P., Hurlburt, H. E., Smedstad, O. M., Halliwell, G. R., Hogan, P. J., Wallcraft, A. J., et al. (2007). The HYCOM (hybrid coordinate ocean model) data assimilative system. *Journal of Marine Systems*, 65(1–4), 60–83. <https://doi.org/10.1016/j.jmarsys.2005.09.016>
- Chin-Bing, S. A., King, D. B., Murphy, J. E., & Li, G. (1994). Long-range cw and time-domain simulations of ocean acoustic scatter from Mid-Atlantic Ridge corners. In *Automatic Object Recognition IV* (Vol. 2234, pp. 188–194). International Society for Optics and Photonics.
- Craig, C. H., & Sandwell, D. T. (1988). Global distribution of seamounts from Seasat profiles. *Journal of Geophysical Research: Solid Earth*, 93(B9), 10408–10420. <https://doi.org/10.1029/jb093ib09p10408>
- Devey, Colin, W., & Wölfel, A.-C. (2020). Multibeam bathymetry raw data (Kongsberg EM 122 entire dataset) of RV MARIA S. MERIAN during cruise MSM88/1. GEOMAR - Helmholtz Centre for Ocean Research Kiel. <https://doi.org/10.1594/PANGAEA.919112>
- Egbert, G. D., & Ray, R. D. (2003). Semi-diurnal and diurnal tidal dissipation from TOPEX/Poseidon altimetry. *Geophysical Research Letters*, 30(17). <https://doi.org/10.1029/2003gl017676>
- GEBCO Bathymetric Compilation Group. (2020). The GEBCO\_2020 Grid - a continuous terrain model of the global oceans and land. British Oceanographic Data Centre, National Oceanography Centre. <https://doi.org/10.5285/c6612cbe-50b3-0cff-e053-6c86abc09f8f>
- Gevorgian, J., Sandwell, D. T., Yu, Y., Kim, S.-S., & Wessel, P. (2021). Global distribution and morphology of seamounts, T45D-0273, presented at Fall Meeting. AGU. 13–17 December.
- Gille, S. T., Yale, M. M., & Sandwell, D. T. (2000). Global correlation of mesoscale ocean variability with seafloor roughness from satellite altimetry. *Geophysical Research Letters*, 27(9), 1251–1254. <https://doi.org/10.1029/1999gl007003>
- Goff, J. A. (2010). Global prediction of abyssal hill root-mean-square heights from small-scale altimetric gravity variability. *Journal of Geophysical Research: Solid Earth*, 115(B12). <https://doi.org/10.1029/2010jb007867>
- Goff, J. A. (2020). Identifying characteristic and anomalous mantle from the complex relationship between abyssal hill roughness and spreading rates. *Geophysical Research Letters*, 47(11), e2020GL088162. <https://doi.org/10.1029/2020gl088162>
- Goff, J. A., & Arbic, B. K. (2010). Global prediction of abyssal hill roughness statistics for use in ocean models from digital maps of paleo-spreading rate, paleo-ridge orientation, and sediment thickness. *Ocean Modelling*, 32(1–2), 36–43. <https://doi.org/10.1016/j.ocemod.2009.10.001>
- Goff, J. A., & Jordan, T. H. (1988). Stochastic modeling of seafloor morphology: Inversion of sea beam data for second-order statistics. *Journal of Geophysical Research: Solid Earth*, 93(B11), 13589–13608. <https://doi.org/10.1029/jb093ib11p13589>
- Goff, J. A., & Jordan, T. H. (1989). Stochastic modeling of seafloor morphology: A parameterized Gaussian model. *Geophysical Research Letters*, 16(1), 45–48. <https://doi.org/10.1029/gl016i001p00045>
- Hall, J. K. (2006). GEBCO centennial special issue—charting the secret world of the ocean floor: The GEBCO project 1903–2003. *Marine Geophysical Researches*, 27(1), 1–5. <https://doi.org/10.1007/s11001-006-8181-4>

- Hébert, H., Deplus, C., Huchon, P., et al (2001). Lithospheric structure of a nascent spreading ridge inferred from gravity data: The western Gulf of Aden. *Journal of Geophysical Research*, 106(B1126), 345363–345426.
- Heezen, B. C., Tharp, M., & Ewing, M. (1959). *The floors of the oceans: I. The North Atlantic* (Vol. 65). Geological Society of America.
- Jayne, S. R., & St Laurent, L. C. (2001). Parameterizing tidal dissipation over rough topography. *Geophysical Research Letters*, 28(5), 811–814. <https://doi.org/10.1029/2000gl012044>
- Kim, S., & Wessel, P. (2011). New global seamount census from altimetry-derived gravity data. *Geophysical Journal International*, 186, 615–631. <https://doi.org/10.1111/j.1365-246x.2011.05076.x>
- Kim, S. S., & Wessel, P. (2015). October. Finding seamounts with altimetry-derived gravity data. In *OCEANS 2015-MTS/IEEE Washington* (pp. 1–6). IEEE.
- Loubrieu, B. (2019a). *Bathymetry - Kerguelan Islands (synthesis, 2019) cell size 200 m*. Ifremer. <https://doi.org/10.12770/1909f2fb-09ee-49e3-8b5f-52b12e53d292>
- Loubrieu, B. (2019b). *Bathymetry of the French Guiana margin and Demerara plateau/data compilation*, Ifremer. <https://doi.org/10.12770/1f127956-8350-466e-b795-c8a9eb3c218e>
- Loubrieu, B., Jean-Yves, R., & Marcia, M. (2020). *Bathymetry around Saint-Paul and Amsterdam islands/data compilation 2020*, Ifremer. <https://doi.org/10.12770/342b2892-b0de-4566-bd77-520fb3bf4ea9>
- Mackenzie, K. V. (1961). Bottom reverberation for 530-and 1030-cps sound in deep water. *Journal of the Acoustical Society of America*, 33(11), 1498–1504. <https://doi.org/10.1121/1.1908482>
- Matthews, K. J., Müller, R. D., Wessel, P., & Whittaker, J. M. (2011). The tectonic fabric of the ocean basins. *Journal of Geophysical Research: Solid Earth*, 116(B12). <https://doi.org/10.1029/2011jb008413>
- Mayer, L., Jakobsson, M., Allen, G., Dorschel, B., Falconer, R., Ferrini, V., et al. (2018). The Nippon Foundation—GEBCO seabed 2030 project: The quest to see the world's oceans completely mapped by 2030. *Geosciences*, 8(2), 63. <https://doi.org/10.3390/geosciences8020063>
- Menard, H. W. (1964). *Marine geology of the Pacific*. McGraw Hill.
- Mendel, V., Sauter, D., Patriat, P., & Munschy, M. (2000). Relationship of the Central Indian Ridge segmentation with the evolution of the Rodriguez triple junction for the past 8 Ma. *Journal of Geophysical Research*, 105, 16563–16575. <https://doi.org/10.1029/2000jb900098>
- Parker, R. L. (1973). The rapid calculation of potential anomalies. *Geophysical Journal International*, 31(4), 447–455. <https://doi.org/10.1111/j.1365-246x.1973.tb06513.x>
- Polzin, K. L., Toole, J. M., Ledwell, J. R., & Schmitt, R. W. (1997). Spatial variability of turbulent mixing in the abyssal ocean. *Science*, 276(5309), 93–96. <https://doi.org/10.1126/science.276.5309.93>
- Ruellan, E. North Fiji basin (Southwest Pacific) - 1000m. Ifremer. <https://doi.org/10.12770/f651de98-9478-4d42-9dc9-c0ec7a43ae87>
- Sandwell, D. T., Harper, H., Tozer, B., & Smith, W. H. (2021). Gravity field recovery from geodetic altimeter missions. *Advances in Space Research*, 68(2), 1059–1072. <https://doi.org/10.1016/j.asr.2019.09.011>
- Sandwell, D. T., Müller, R. D., Smith, W. H., Garcia, E., & Francis, R. (2014). New global marine gravity model from CryoSat-2 and Jason-1 reveals buried tectonic structure. *Science*, 346(6205), 65–67. <https://doi.org/10.1126/science.1258213>
- Sandwell, D. T., & Smith, W. H. (2009). Global marine gravity from retracked Geosat and ERS-1 altimetry: Ridge segmentation versus spreading rate. *Journal of Geophysical Research: Solid Earth*, 114(B1). <https://doi.org/10.1029/2008jb006008>
- Sauter, D., & Mendel, V. (2000). *The Southwest Indian ridge between 65°E and 68°E-120m*. Ifremer. <https://doi.org/10.12770/e54561cf-a7aa-4336-a935-7cfec6e1cdbb>
- Scott, R. B., Goff, J. A., Naveira Garabato, A. C., & Nurser, A. J. G. (2011). Global rate and spectral characteristics of internal gravity wave generation by geostrophic flow over topography. *Journal of Geophysical Research: Oceans*, 116(C9). <https://doi.org/10.1029/2011jc007005>
- Sepúlveda, I., Tozer, B., Haase, J. S., Liu, P. L. F., & Grigoriu, M. (2020). Modeling uncertainties of bathymetry predicted with satellite altimetry data and application to tsunami hazard assessments. *Journal of Geophysical Research: Solid Earth*, 125(9), e2020JB019735.
- Seton, M., Müller, R. D., Zahirovic, S., Williams, S., Wright, N. M., Cannon, J., et al. (2020). A global data set of present-day oceanic crustal age and seafloor spreading parameters. *Geochemistry, Geophysics, Geosystems*, 21(10), e2020GC009214. <https://doi.org/10.1029/2020gc009214>
- Sisavath, E., Babonneau, N., Saint-Ange, F., Bachélery, P., Jorry, S. J., Deplus, C., et al. (2011). Morphology and sedimentary architecture of a modern volcanoclastic turbidite system: The Cilaos fan, offshore La Réunion Island. *Marine Geology*, 288(1–4), 1–17. <https://doi.org/10.1016/j.margeo.2011.06.011>
- Sjöberg, L. E. (2005). A discussion on the approximations made in the practical implementation of the remove–compute–restore technique in regional geoid modelling. *Journal of Geodesy*, 78(11–12), 645–653.
- Smith, D. (1988). Shape analysis of Pacific seamounts. *Earth and Planetary Science Letters*, 90, 457–466. [https://doi.org/10.1016/0012-821x\(88\)90143-4](https://doi.org/10.1016/0012-821x(88)90143-4)
- Smith, D., & Jordan, T. (1988). Seamount statistics in the Pacific ocean. *Journal of Geophysical Research*, 94(B4), 2899–2918. <https://doi.org/10.1029/jb093ib04p02899>
- Smith, W. H., & Sandwell, D. T. (1994). Bathymetric prediction from dense satellite altimetry and sparse shipboard bathymetry. *Journal of Geophysical Research: Solid Earth*, 99(B11), 21803–21824. <https://doi.org/10.1029/94jb00988>
- Smith, W. H. F., & Wessel, P. (1990). Gridding with continuous curvature splines in tension. *Geophysics*, 55(3), 293–305. <https://doi.org/10.1190/1.1442837>
- Staudigel, H., Koppers, A., Lavelle, W., et al. (2010). Defining the word “seamount”. *Oceanography*, 23(No 1), 20–21. <https://doi.org/10.5670/oceanog.2010.85>
- Straume, E. O., Gaina, C., Medvedev, S., Hochmuth, K., Gohl, K., Whittaker, J. M., et al. (2019). GlobSed: Updated total sediment thickness in the world's oceans. *Geochemistry, Geophysics, Geosystems*, 20(4), 1756–1772. <https://doi.org/10.1029/2018gc008115>
- Talbot, S., & Loubrieu, B. Retrieved from <https://w3.ifremer.fr/archimer/doc/00613/72480/https://sextant.ifremer.fr/eng/Data/Catalogue#/meta-data/915d04a1-220f-4784-934c-c269a515e5a9>
- Timko, P. G., Arbic, B. K., Goff, J. A., Ansong, J. K., Smith, W. H., Melet, A., & Wallcraft, A. J. (2017). Impact of synthetic abyssal hill roughness on resolved motions in numerical global ocean tide models. *Ocean Modelling*, 112, 1–16. <https://doi.org/10.1016/j.ocemod.2017.02.005>
- Tozer, B., Sandwell, D. T., Smith, W. H., Olson, C., Beale, J. R., & Wessel, P. (2019). Global bathymetry and topography at 15 arc sec: SRTM15+. *Earth and Space Science*, 6(10), 1847–1864. <https://doi.org/10.1029/2019ea000658>
- Watts, A. B., Sandwell, D. T., Smith, W. H. F., & Wessel, P. (2006). Global gravity, bathymetry, and the distribution of submarine volcanism through space and time. *Journal of Geophysical Research*, 111(B8). <https://doi.org/10.1029/2005JB004083>
- Wessel, P. (1997). Sizes and ages of seamounts using remote sensing: Implications for intraplate volcanism. *Science*, 277, 802–805. <https://doi.org/10.1126/science.277.5327.802>
- Wessel, P. (2001). Global distribution of seamounts inferred from gridded Geosat/ERS-1 altimetry. *Journal of Geophysical Research: Solid Earth*, 106(B9), 19431–19441. <https://doi.org/10.1029/2000jb000083>

- Wessel, P., Luis, J. F., Uieda, L., Scharroo, R., Wobbe, F., Smith, W. H. F., & Tian, D. (2019). The generic mapping tools version 6. *Geochemistry, Geophysics, Geosystems*, 20(11), 5556–5564. <https://doi.org/10.1029/2019gc008515>
- Wessel, P., Sandwell, D., & Kim, S. (2010). The global seamount census. special issue on mountains in The sea. *Oceanography*, 23(1), 24–33. <https://doi.org/10.5670/oceanog.2010.60>
- Wölfel, A.-C., & Devey, C. W. (2020). Multibeam bathymetry raw data (Kongsberg EM 122 entire dataset) of RV MARIA S. MERIAN during cruise MSM88/2. GEOMAR - Helmholtz Centre for Ocean Research Kiel. <https://doi.org/10.1594/PANGAEA.918716>
- Yesson, C., Clark, M. R., Taylor, M. L., & Rogers, A. D. (2011). The global distribution of seamounts based on 30 arc seconds bathymetry data. *Deep Sea Research Part I: Oceanographic Research Papers*, 58(4), 442–453. <https://doi.org/10.1016/j.dsr.2011.02.004>